JOURNAL OF SOLID STATE CHEMISTRY 114, 317–325 (1995)

EXAFS Structure and Electrical Properties of Lithium Niobium Phosphate

S. Bruque,*[1] M. Martinez Lara,* L. Moreno,* T. Ramirez-Cárdenas,* J. Chaboy,†[,2] M. Marziali,‡ and S. Stizza‡

*Departmento de Química Inorgánica, Universidad de Málaga, apdo. 59, 29071 Málaga, Spain; †INFN Laboratori Nazionali di Frascati, Italy; and ‡Dipartimento di Matematica e Fisica, Università di Camerino, 62032 Camerino, Italy

Received March 4, 1993; in revised form March 14, 1994; accepted March 18, 1994

The acidic character of the hydration water in $NbOPO_4 \cdot 2H_2O$ permits the exchange of protons for Li^+ ions. The lithium phase annealed at 773 K presents a slightly distorted lattice with respect to the niobium phosphate network, allowing high mobility of the lithium ion. The structural modifications due to Li insertion have been studied by extended X-ray absorption spectroscopy (EXAFS) at the Nb *K*-edge. The analysis of the EXAFS spectra indicates the presence of an additional oxygen atom close to Nb which is probably not bonded to the framework. The ionic conductivity of the $LiNb(OH)OPO_4$ phase is high and increases up to 880 K. At higher temperatures, the Li^+ ion migrates to a permanent position in the network and the ionic conductivity is then stopped.

INTRODUCTION

Superionic conductors are solid materials with high ionic conductivities (10^{-1}–10^{-4} $\Omega^{-1}cm^{-1}$) comparable with those of liquid electrolytes. The mobile ions could be Na^+ as in Na–β-Al_2O_3, Li^+ as in $Li_{14}ZnGe_4O_{16}$, Ag^+ in α-AgI, or Cu^+ as in $Rb_4Cu_{16}I_7Cl_{13}$ (1). These materials are also characterized by open structures with negligible electronic conductivity. In the search for new solid electrolytes, insulator framework structures permeated by open channels may provide pathways for easy ionic transport. Niobyl phosphate offers such an insulator host structure adequate for ion mobility when its precursor, α-$NbOPO_4 \cdot nH_2O$ ($n \leq 3$), is doped with light ions by solid-state reactions.

Lithium intercalates are very promising materials for high-energy-density batteries because of their high electrochemical potential and ionic mobility (2–4). We present here a structural study using X-ray diffraction (XRD) and extended absorption X-ray spectroscopy (EXAFS) of the lithium niobium phosphates and their electrochemical properties.

[1] To whom correspondence should be addressed.

[2] Present address: Departamento de Física de la Materia Condensada & Instituto de Ciencia de Aragón U.E.I.V., CSIC-Universidad de Zaragoza, 50009 Zaragoza, Spain.

The chemical strategy for the preparation of an ionic conductor by lithium ion insertion into the channels of the $NbOPO_4$ framework is to begin with an open-layer lattice (niobyl phosphate hydrate), to energize the water molecules by partial dehydration, then to exchange the proton from the residual acid water with lithium, and finally to complete the dehydration and so provoke the collapse of the structure (2D → 3D).

In order to locate the perturbation provoked by the lithium atoms in our system, we have performed X-ray absorption experiments at the *K*-edge of niobium in $NbOPO_4$ and $NbOPO_4 \cdot 2H_2O$, as well as in their lithium-doped derivatives $LiOHNbOPO_4$ and $LiOHNbOPO_4 \cdot 2H_2O$.

EXPERIMENTAL

A. Preparation and Characterization of Lithium Niobium Phosphates

$NbOPO_4 \cdot 2H_2O$ was used as a starting reactant and was prepared following the method given in a previous paper (5). The lithium insertion was studied by bringing $NbOPO_4 \cdot 2H_2O$ into contact with lithium chloride at 473 K for a week. Experiments were performed using different molar ratios Li : Nb in the insertion process: 0.25, 0.5, 1, and 1.5. The resulting solids were washed with methanol, then separated by centrifugation and air-dried. These solids are hydrated, but dehydration becomes irreversible near 700 K. The conductivity measurements were obtained from annealed solids at 773 K for 12 hr.

To determine the chemical composition of the solids, they were dissolved in fused KOH for the lithium derivatives or by dissolution in hydrofluoric acid for the pristine solid. Niobium was determined by precipitation of the corresponding cupferron complex and subsequent calcination to oxide at 1273 K. Phosphorus was analyzed by colorimetric analysis through the blue molybdophosphate complex. The lithium content was obtained by flame emission spectrometry. X-ray diffraction was performed on the powders with a Siemens D501 automated diffrac-

0022-4596/95 $6.00

tometer using graphite-monochromated Cu$K\alpha$ radiation. Thermal analyses (TGA and DTA) were carried out on a Rigaku Thermoflex instrument. The samples were heated in air at a rate of 10 K · min^{-1} with calcined Al_2O_3 as the reference standard. The diffuse-reflectance spectra were obtained on a Shimadzu UV-3100 UV-visible-near-IR instrument, using an integrating sphere and $BaSO_4$ as a blank reference.

B. Conductivity Measurements

Pellets, of 13 mm diameter and 1.5 mm thickness, were prepared by pressing 500 mg of material at 6 MPa and then sintering at 773 K overnight. Pellets were placed between two gold electrodes.

The ac complex impedance measurements were performed in air using a Solartron FRA 1255 and an electrochemical-interface Solartron 1286 controlled by a computer. The temperature range used was 490–881 K and the frequency range was 1 Hz–2 MHz. Corresponding measurements of electrical properties were made beginning from high frequencies and high temperatures and moving to low values of these parameters.

C. EXAFS Measurements

The X-ray absorption measurements were performed using the laboratory XAFS facility of the Centro Interdipartimentale Grandi Apparecchiature (CIGA) at Camerino University (Italy). The spectrometer used consists of a Johansson-cut bent crystal, a rotating anode X-ray generator (Rigaku RU-200, 12 kW), and a fast detection system using a solid state detector (SSD)(6, 7). The absorption spectra were recorded at room temperature, in the transmission set–reset mode, using a Ge(440) crystal monochromator; X-ray intensities were measured in the direct mode, i.e., with the sample in and out of the beam at each energy point, using a pure-Be SSD Canberra GL0213R detector. During the measurements, the voltage and current of the Mo rotating-anode X-ray generator were 20 KeV and 100 mA, respectively, and the discrimination window was optimized to avoid any contribution of the Mo$K\beta_1$ (19608.3 eV) emission line to the spectra.

Samples were prepared by pulverizing the materials and then spreading the fine powders on an adhesive tape. Several layers were used to obtain an absorption jump of $\Delta\mu x \approx 1.5$ for each compound.

RESULTS AND DISCUSSION

1. Lithium Derivatives and Their Properties

The water molecule coordinated to the niobium atom of $NbOPO_4 \cdot H_2O$ has acid behavior:

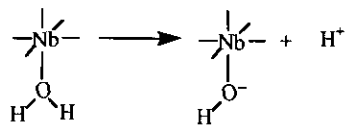

The mechanism proposed for the lithium insertion into $NbOPO_4 \cdot H_2O$ is ion exchange and interdiffusion of H^+/Li^+ in its interlayer space favored by the generation and release of HCl. Thus, the hydrogen belonging to the coordianted water of the niobium can be exchanged with lithium, as shown in Eq. [1]:

$$x\mathrm{Li^+(LiCl)} + \mathrm{NbOPO_4 \cdot H_2O} \xrightarrow{473\ \mathrm{K}} (\mathrm{LiOH})_x\mathrm{NbOPO_4} \cdot (1-x)\mathrm{H_2O} + \mathrm{HCl} \quad [1]$$

We have considered $NbOPO_4 \cdot H_2O$ as the reactant at the reaction temperature though $NbOPO_4 \cdot 2H_2O$ was used as raw material. The monohydrate is the most stable phase against $NbOPO_4 \cdot 2H_2O$ at 473 K.

Attempts were made to achieve a lithium insertion in the anhydrous α-$NbOPO_4$ by ceramic methods, but they failed due to the absence of reactive sites in this solid. The amounts of lithium in the ceramic solids were very low and their conductivities were similar to that of the pristine solid (α-$NbOPO_4$).

The composition of the obtained solids are summarized in Table 1. The diffractograms of the lithium compounds annealed at 773 K have a similar profile to that of anhydrous $NbOPO_4$, but the diffraction lines are wider and hence the precision in the interplanar spacings is poorer. It is not possible to index correctly the diffractograms of these materials; therefore we have resorted to an EXAFS study at the *K*-edge of niobium to attempt to locate the lithium ion through its influence in the environment of niobium. The crystallographic data indicate that the *ab* plane of the pristine framework is well preserved in the lithium phases, which adopt the same tetragonal structure.

The electronic absorption spectra for the lithium derivatives and the $NbOPO_4$ host are slightly different with an absorption band around 255 nm in the UV–visible region that is characteristic of an $L \rightarrow M$ charge transfer. This

TABLE 1
Composition Data for $(LiOH)_nNbOPO_4$ Compounds

Li:Nb in the reaction	Composition
0.25	$(LiOH)_{0.2}NbOPO_4$
0.50	$(LiOH)_{0.4}NbOPO_4$
1.00	$(LiOH)_{0.9}NbOPO_4$
1.50	$(LiOH)_{1.0}NbOPO_4$

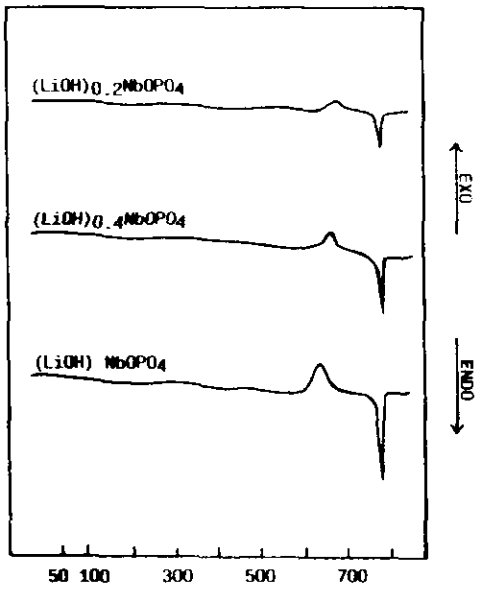

FIG. 1. DTA curves of $Li(OH)_xNbOPO_4$.

band for the lithium derivatives is wider than the corresponding one in the α-$NbOPO_4$. This can be explained if it is assumed that the lithium insertion in the lattice produces a disturbance about the [NbO_6] octhahedra which is observed in the EXAFS spectra.

Differential thermal analyses (DTA) confirm semiquantitatively the lithium injected into the $NbOPO_4$ network (Fig. 1). A noticeable characteristic of these solids is the relationship between the lithium content and the intensity of two thermal effects; one exothermic around 933 K and the other endothermic at 1053 K. These effects occur without loss of mass, which indicates some kind of structural transformation. The temperature of the exothermic effect decreases as the lithium content increases but no changes are observed with XRD. The transformation is probably associated with the energy change involved with the anchorage of Li^+ into the lattice: the lithium mobility becomes negligible for samples sintered at those temperatures ($T > 930$ K). The temperature of the endothermic effect remains unaltered for all the lithium derivatives. When the lithium niobium phosphate is heated to 1053 K structural modifications are observed. The diffraction profile is very complex with a great number of peaks, which is characteristic of a multicomponent system. Among them Li_3PO_4 and α-$NbOPO_4$ could be clearly detected as major components due to a lithium diffusion process and a subsequent phase segregation.

2. *Structural Characterization by EXAFS*

Because it is difficult to characterize Li atoms, since their response to the standard structural probes is generally small, it is necessary to use an indirect method to gain insight about Li location in this framework. To this end, we have studied by EXAFS the structural modifications which occurred in the local environment around Nb upon Li introduction. Therefore, instead of looking directly for the presence of Li atoms we have tried to detect the presence of the oxygen of the OH^- group linked to Li in $LiOHNbOPO_4$ and $LiOHNbOPO_4 \cdot 2H_2O$ compounds.

To this end we have made an extensive analysis of the EXAFS signals at the Nb K-edge in $NbOPO_4$ and $NbOPO_4 \cdot 2H_2O$ and their Li derivatives. During the data analysis and in order to achieve the reliability of the structural analysis we have used the precursor compounds, $NbOPO_4$ and $NbOPO_4 \cdot 2H_2O$, as references because both systems are well characterized crystallographically (8).

The raw absorption spectra recorded at the Nb K-edge for the $NbOPO_4$ and $LiOHNbOPO_4$ compounds, as well as for their hydrates, are shown in Fig. 2. Spectra were analyzed according to standard procedures (9): the background contribution from previous edges $\mu_B(E)$ was fitted with a linear function and substracted from the experimental spectrum $\mu(E)$. The average absorption above the edge was fitted with a smooth spline formed by three cubic polynomials to simulate the atomic-like term $\mu_0(E)$. The EXAFS signal $\chi(\mathbf{k})$ was then determined as $\chi(\mathbf{k}) = (\mu - \mu\beta - \mu_0)/\mu_0$, where the photoelectron wave vector $\mathbf{k}$ is defined as $\mathbf{k} = [(2m/\hbar^2)(E - E_0)]^{1/2}$. The energy origin E_0 corresponding to the continuum threshold was defined to be at the inflection point of the absorption edge.

The Fourier transforms (FT) of the EXAFS oscillations obtained in this way are reported in Fig. 3 for both the $NbOPO_4$ and the $NbOPO_4 \cdot 2H_2O$ compounds (10). In both cases, the introduction of lithium does not produce any substantial modification (other than a slight increase in the structural disorder) in the main peak of the FT that corresponds to the contribution to the EXAFS spectra of the oxygen octahedra surrounding the Nb central atom. However, large differences are found in the region between 2 and 4 Å, corresponding to the contribution of the PO_4 tetrahedra. In particular, the FT of both LiOH $NbOPO_4$ and $LiOHNbOPO_4 \cdot 2H_2O$ compounds exhibit an additional contribution at $R \approx 3.5$ Å that is not detected in the FT of precursor compounds. These results evidence that the introduction of Li and the OH group leads to similar modifications in the EXAFS spectra; thus their spatial location must be near the same for both $LiOHNbOPO_4$ and the layered compound LiOH $NbOPO_4 \cdot 2H_2O$.

The determination of the modifications of the local environment of Nb upon Li inclusion in these systems has been carried out by performing theoretical ab initio calcu-

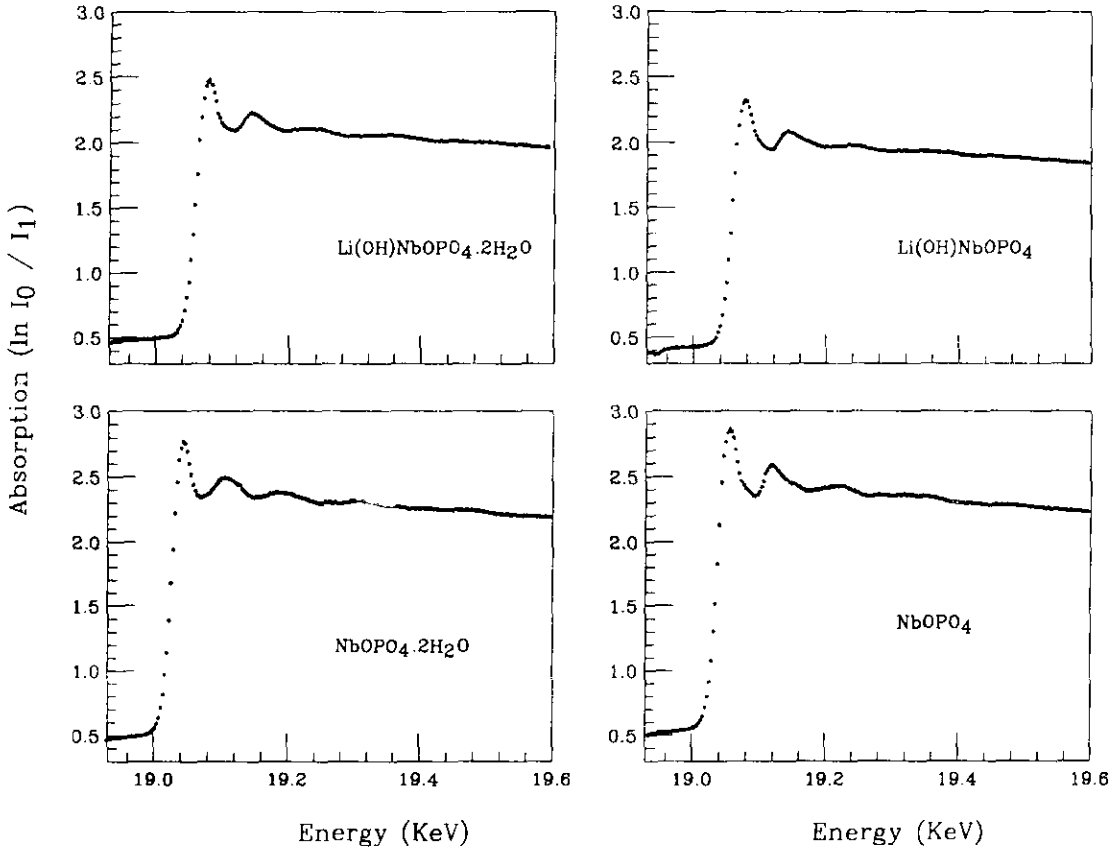

FIG. 2. Experimental X-ray absorption spectra at the Nb K-edge in the $NbOPO_4$, $LiOHNbOPO_4$, $NbOPO_4 \cdot 2H_2O$, and $LiOHNbOPO_4 \cdot 2H_2O$ compounds.

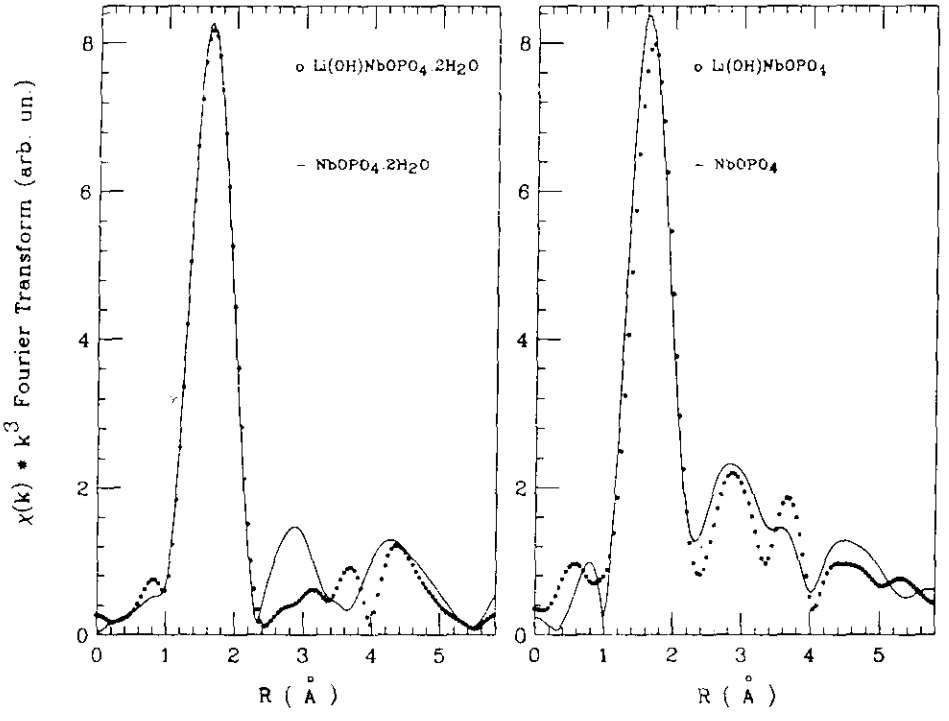

FIG. 3. In the right panel, the comparison of the modulus of the Fourier transform, in arbitrary units, of the experimental EXAFS spectra of $NbOPO_4$ (continuous line) and $LiOHNbOPO_4$ (points) is shown. The Fourier transform was performed in the range 4–12 $Å^{-1}$ for the k^3-weighted spectra, using a Gaussian window. In the left panel the same comparison is shown for $NbOPO_4 \cdot 2H_2O$ and $LiOHNbOPO_4 \cdot 2H_2O$ compounds.

lations of the EXAFS spectra. EXAFS simulations were carried out applying the code EXCURV 88 (11), which is based upon the spherical wave theory developed by Lee and Pendry (12) incorporating the fast curved-wave method (13) to reduce the computational time. The quality of the theoretical simulations was assessed by visual comparison of the experimental and simulated EXAFS spectra and their FT and by the calculation of the fitting index (14) defined, in the program EXCURV88 as

$$\mathrm{FI} = \frac{1}{(100\ \mathrm{NPT})} \sum_{i=1}^{\mathrm{NPT}} (\mathrm{Res}_i\ \mathbf{k}^{\mathrm{WT}})^2,$$

where Res_i = residual$_i$ = χ_i (calculated) − χ_i(experimental) and NPT = number of data points. WT is an integral weight which is used to offset the decay of X as the energy increases. Also, phase shifts are more accurate at high **k** and errors in defining the energy zero, represented in EXCURV88 by the parameter E_0, are also less significant.

Atomic phase shifts and back-scattering factors were calculated approximating the excited niobium atom to the neutral molybdenum atom with one electron removed from the 1*s* level (Z + 1 approximation). Throughout the analysis, **k**-cubed weighting was applied, to compensate for the diminishing amplitude at high **k** and to determine the experimental spectrum shift, E_0 = 22.45 eV, needed to match with the theoretical simulation.

The data analysis was initiated with the precursor $NbOPO_4$, which has been well characerized by X-ray diffraction. The knowledge of the crystal structure of the reference allows us to fix the coordination numbers and to use the same values during the analysis of the hydrated and lithium-doped derivatives as were determined for the reference compounds for E_0 and S_0^2, the empirical corrections for photoelectron shake-up and shake-off, which are strongly correlated with the structural parameters. In this way the only parameters that have been allowed to vary in the refinement process are the interatomic distances and the Debye–Waller factors.

The comparison between the calculated and experimental EXAFS signals for the first coordination shell of Nb is shown in Figs. 4 and 5 for the four compounds under study. The structural parameters obtained from the fit to the theoretical simulations are summarized in Table 2 where the coordination numbers, interatomic distances, and Debye–Waller exponents, σ^2, are also shown. The best fits have been obtained when we include as input parameters three oxygen shells, two of which correspond to the apical-oxygen distances of the distorted octahedron and the other of which corresponds to the plane. Moreover, in the case of the Li compounds, it has been necessary to include a new oxygen located be-

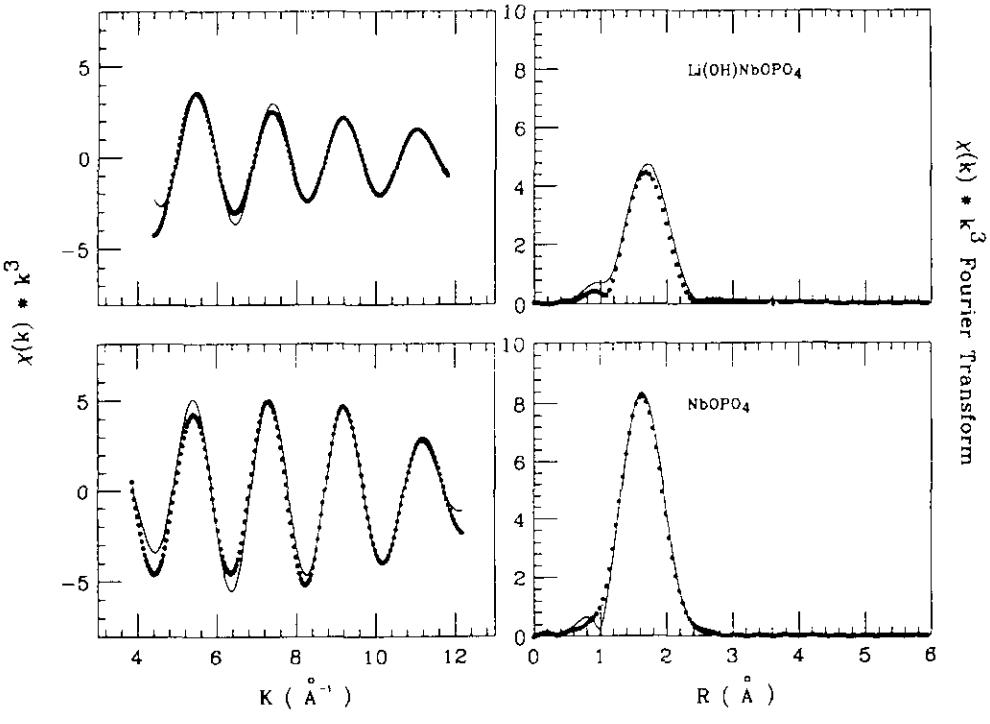

FIG. 4. EXAFS (left) and Fourier transform (right) of the $\mathbf{k}^3$-weighted simulation of the first shell of $NbOPO_4$ (bottom panel) and $LiOHNbOPO_4$ (upper panel). The points correspond to the best fit for elongated octahedra using the structural parameters summarized in Table 2.

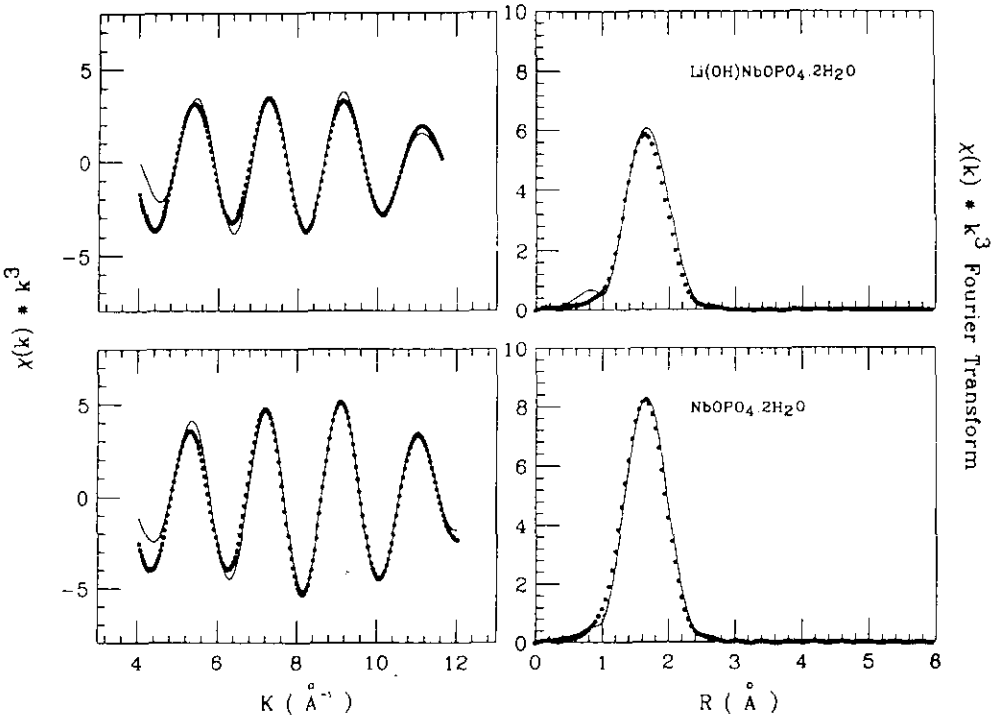

FIG. 5. EXAFS (left) and Fourier transform (right) of the k^3-weighted simulation of the first shell of $NbOPO_4 \cdot 2H_2O$ (bottom panel) and $LiOHNbOPO_4 \cdot 2H_2O$ (upper panel). The points correspond to the best fit for elongated octahedra using the structural parameters summarized in Table 2.

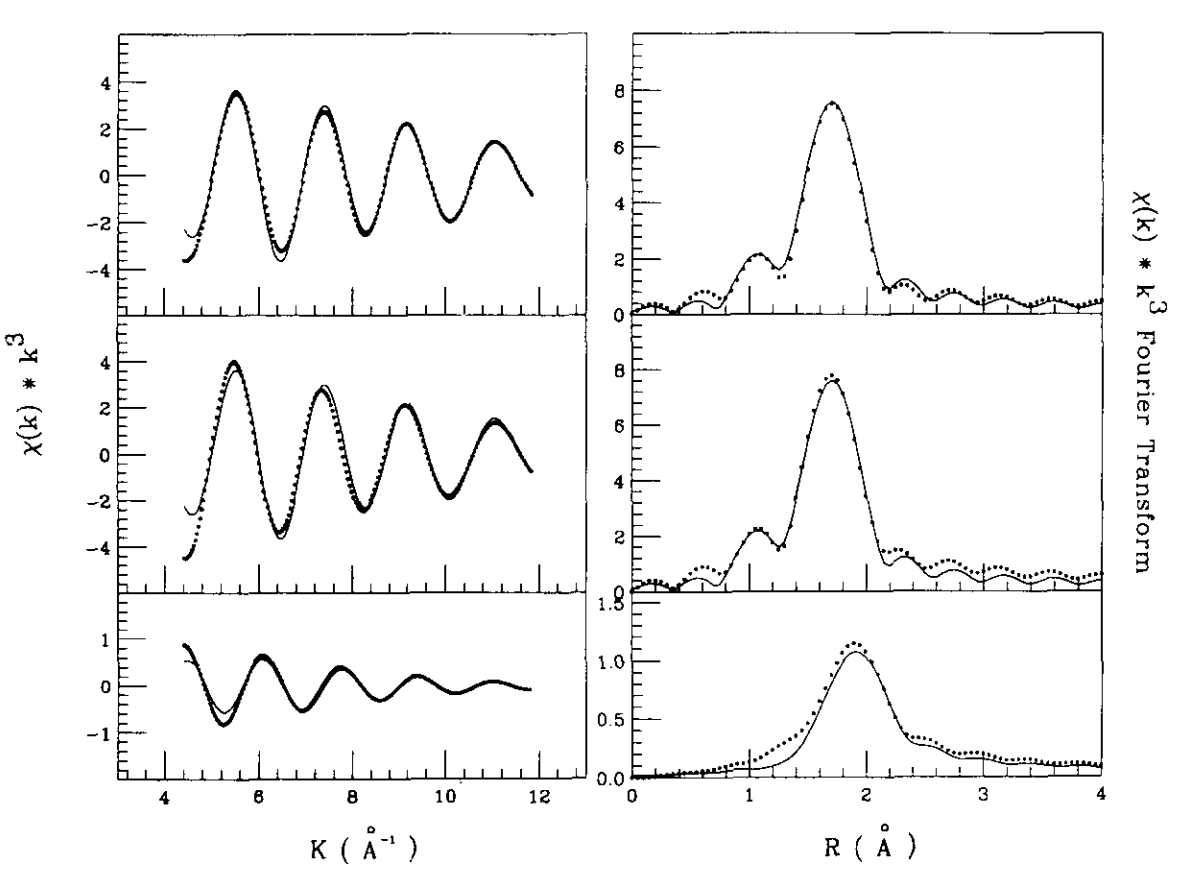

FIG. 6. EXAFS (left) and Fourier transform (right) of the k^3-weighted simulation of the first shell of $LiOHNbOPO_4$. The points correspond to the best fit for elongated octahedra including a new oxygen located between the first oxygen octahedron and the PO_4 tetahedra surrounding the Nb central atom (upper panel) and removing this last contribution (middle panel). In the bottom panel the EXAFS difference signal and its fit to a Nb–O path are shown.

tween the first oxygen octahedron and the PO_4 tetrahedra surrounding the Nb central atom. The high Debye–Waller factor associated with this atom indicates its great mobility, as expected for the nonbonded OH^- group.

Notwithstanding the remarkable agreement between the theoretical simulations and the experimental EXAFS signals, we have applied the difference EXAFS data analysis technique (15) to verify the reliability of the presence of a new oxygen atom near the central Nb. According to this method, we have fixed the theoretical contribution of the oxygen octahedron and subtracted it from the experimental EXAFS spectrum. Then, the difference found is analyzed as corresponding to a single Nb–O scattering path. The results, shown in Figs. 6 and 7, seem to validate the structural hypothesis derived from the direct analysis of the EXAFS spectra.

As discussed above, the framework of niobyl phosphate is quite well-preserved after intercalation although the extra oxygen (at 2.25 Å of Nb, see Table 2) would open the structure making the X-ray pattern broader. The insertion may create voids between the PO_4 and NbO_6 groups where the extra oxygen atoms should be located. This open process generates empty spaces where lithium ions are situated.

3. Electrical Conductivity

In Fig. 8 we can see the Nyquist plot at 780 K for the lithium derivative with the highest lithium content, Li $Nb(OH)OPO_4$. There are two arcs and the electrode–sample interface response characteristic of an ionic conductor (14). The first arc, low frequency, is due to the grain boundary interface resistance and the high-frequency arc is related to the bulk resistance. The equivalent circuit (Fig. 8) consists of two subcircuits, one corresponding to the bulk conduction process and the other to the grain boundary effects. The former is an $R(QC)$ system, where Q is a constant phase element (CPE) $Q(\omega) = A(i\,\omega)^{-n}$, A is the impedance, ω is the angular frequence, and n is an empirical parameter related to the dielectric rigidity of the system, whose value is $0 < n \leq 1$. For all temperatures from 490 to 881 K we can calculate the

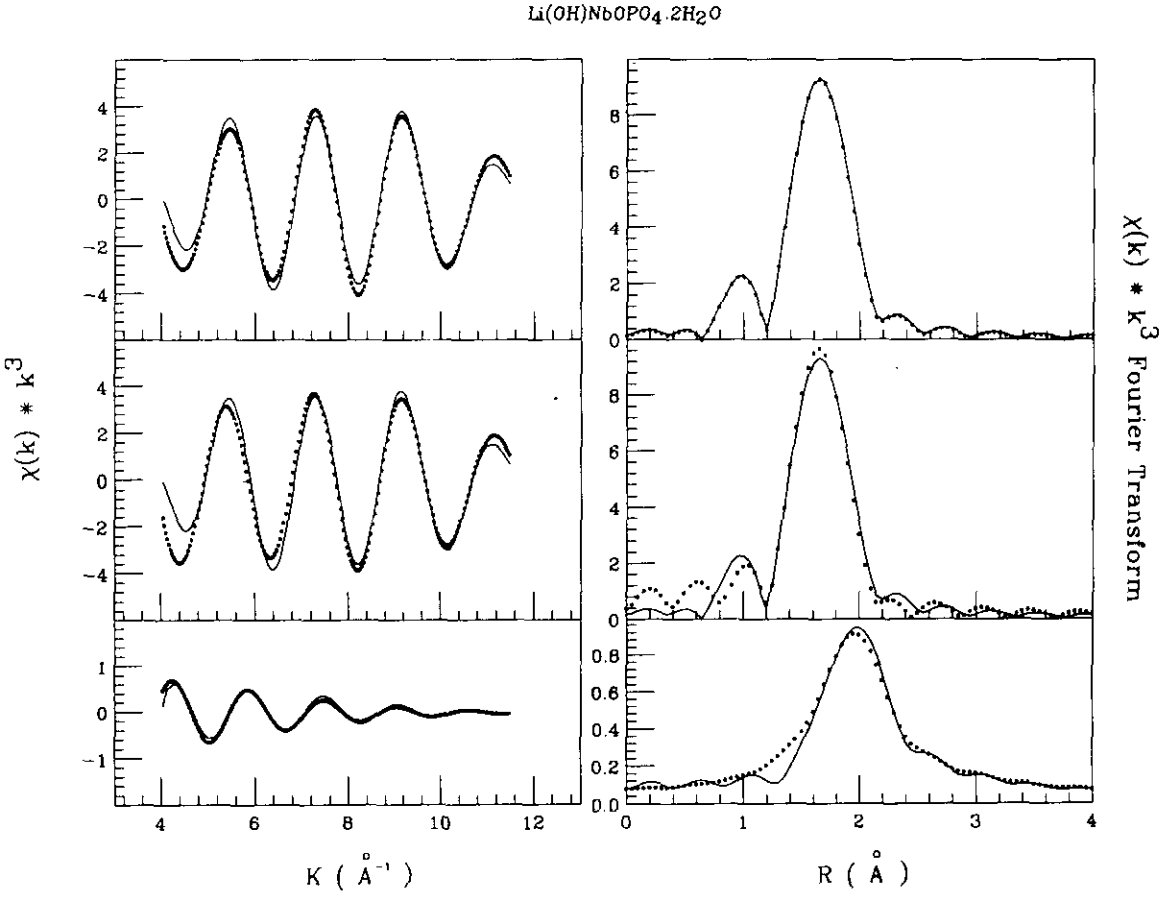

FIG. 7. EXAFS (left) and Fourier transform (right) of the k^3-weighted simulation of the first shell of $LiOHNbOPO_4 \cdot 2H_2O$. The points correspond to the best fit for elongated octahedra and including a new Nb–O contribution (upper panel) and removing this last contribution (middle panel). In the bottom panel the analysis of the EXAFS difference signal is shown.

TABLE 2

Radial Distribution about the Nb Atom and Structural Parameters Obtained from EXAFS and X-Ray Diffraction (XRD) Analyses for Solids Annealed at 773 K and Air-Dried (Dihydrates)

	$NbOPO_4$ (FI = 0.76)				$Li(OH)NbOPO_4$ (FI = 0.35)		
	N	R (Å)	$2\sigma^2$ (Å^2)	XRD Ref. (8)	N	R (Å)	$2\sigma^2$ (Å^2)
O	1	1.67	0.009	1.783	1	1.72	0.010
O	4	1.94	0.009	1.969	4	1.94	0.014
O	1	2.34	0.010	2.321	1	2.31	0.013
O	—	—	—	—	1	2.25	0.025
	$NbOPO_4 \cdot 2H_2O$ (FI = 0.59)				$Li(OH)NbOPO_4 \cdot 2H_2O$ (FI = 0.78)		
	N	R (Å)	$2\sigma^2$ (Å^2)		N	R (Å)	$2\sigma^2$ (Å^2)
O	1	1.68	0.008		1	1.68	0.010
O	4	1.97	0.009		4	1.95	0.012
O	1	2.33	0.010		1	2.34	0.012
O	—	—	—		1	2.31	0.020

electrical conductivity by the small arc extrapolation to the real impedance axis.

Of the lithium derivatives, $LiNb(OH)OPO_4$ logically presents the highest conductivity since it has a greater number of lithium carriers for the motion. This fact suggests that the dominant conducting species are alkali cations. This ionic conductor showed a conductivity of 0.9×10^{-4} S · cm^{-1} at 856 K against 10^{-12} S · cm^{-1} for the pristine solid α-$NbOPO_4$, with an activation energy of

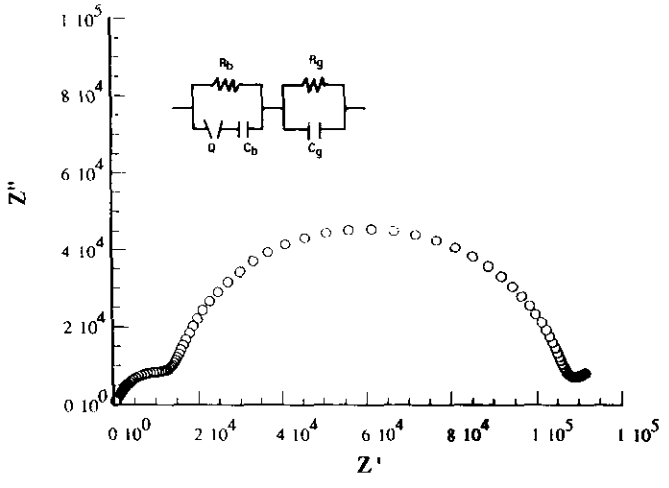

FIG. 8. The Nyquist plot for $LiOHNbOPO_4$ at 780 K. The subscript b refers to the bulk and subscript g refers to the grain boundary effects in the equivalent circuit.

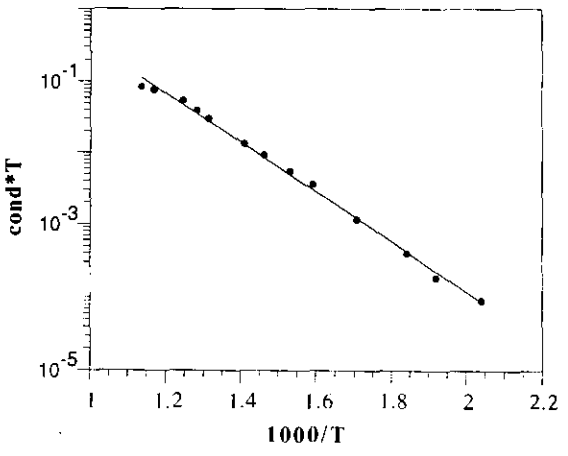

FIG. 9. The Arrhenius plot for $LiOHNbOPO_4$.

0.66 eV which was derived from the Arrhenius plot (Fig. 9). The relatively large activation energy required for the conduction of Li^+ ions in the material may be related to the CPE in which n ranges between 0.3 and 0.4. When $n = 0.5$ the conduction process is a diffusive type according to Fick's law, but in our case a hindered diffusion could take place. According to the EXAFS study, the Nb environment has been slightly modified toward a more open structure, but the framework does not allow well-defined channels. Li^+ mobility in the empty spaces becomes possible, but the mechanism involved in the ion conduction is not purely diffusive.

CONCLUSIONS

The $NbOPO_4$ framework has been revealed to be appropiate for lithium intercalation in its channels. To facilitate the lithium diffusion and its exchange, the reaction was made with an accessible lamellar precursor and afterward the network was collapsed toward a 3D system. The EXAFS analysis supports that Li uptake in the $NbPO_4$ framework induces a distortion around Nb atoms showing a seven-oxygen coordination in which the extra oxygen coming from the inserted lithium hydroxide is not bonded to the framework. According to this structural configuration, the Li ion should exhibit a high mobility, in agreement with the high values of ionic conductivity found.

ACKNOWLEDGMENTS

We thank R. Marassi for the use of the CIGA Laboratory EXAFS facility in which to perform the X-ray absorption measurements.

REFERENCES

1. T. Kudo and K. Fueki, "Solid State Ionics", Chapter 6 Kodansha-VCH, Tokyo, 1990.
2. Y. Yong and P. Wengin, *Mater. Res. Bull.* **25,** 841 (1990).
3. P. Hagenmuller and C. Delmas, *Mater. Res. Soc. Symp. Proc.* **210,** 323 (1991).
4. R. West, B. Zachau-Christiansen, T. Jacobsen, and S. Skaarup, *Mater. Res. Soc. Symp. Proc. 210,* 449 (1991).
5. S. Bruque, M. Martinez, L. Moreno, A. Jimenez, B. Casal, E. Ruiz-Hitzky, and J. Sanz, *Inorg. Chem.* **26,** 847 (1987).
6. K. Tohji and Y. Udagawa, *Jpn. J. Appl. Phys.* **22**(5), 882 (1983).
7. K. Tohji, Y. Udagawa, T. Kawasaki, and K. Masuda, *Rev. Sci. Instrum.* **54**(11), 1482 (1983).
8. J. M. Longo and P. Kierkegaard, *Acta Chem. Scand. 20,* 72 (1966).
9. See, for example, "X-Ray Absorption: Principles, Applications, Techniques of EXAFS, SEXAFS and XANES," (D. C. Kronisberger and R. Prins, Eds.), J. Wiley, New York, 1986.
10. Note that the phase correction was not included in the Fourier transform, therefore the peak positions are shifted from their true values. C. A. Ashley and S. Doniach, *Phys. Rev. B: Condens. Matter* **11,** 1279 (1975).
11. N. Binsted, S. J. Gurman, and S. Campbell, SERC Daresbury Laboratory, (SERC Daresbury Laboratory, Program EXCURV 88, (1988).
12. P. A. Lee and J. B. Pendry, *Phys. Rev. B: Condens. Matter* **119,** 2795 (1975).
13. S. J. Gurman, N. Binsted, and I. Ross, *J. Phys. C* **7,** 143 (1984).
14. Report of the International Workshop on Standards and Criteria in X-Ray Absorption Spectroscopy, *Physica B* **158,** 701 (1989).
15. S. S. Hasnain, *in* "Biophysics and Synchrotron Radiation" (A. Bianconi and A. Congiu Castellano, Eds.). (Springer-Verlag, Berlin, 1987.)